Journal of Alloys and Compounds 850 (2021) 156671

Contents lists available at ScienceDirect

Journal of Alloys and Compounds

journal homepage: http://www.elsevier.com/locate/jalcom

Bio-synthesised black α-Cr_2O_3 nanoparticles; experimental analysis and density function theory calculations

J. Sackey [a, b, c, d, *], R. Morad [a, b], A.K.H. Bashir [a, b], L.Kotsedi [a, b, e], C.Kaonga [c], M. Maaza [a, b]

[a] Nanosciences African Network (NANOAFNET), iThemba LABS-National Research Foundation, Old Faure Road, 7129, Somerset West, South Africa
[b] UNESCO-UNISA Africa Chair in Nanosciences/Nanotechnology, College of Graduate Studies, University of South Africa (UNISA), Muckleneuk Ridge, P.O. Box 392, Pretoria, South Africa
[c] University of Malawi, The Polytechnic, Private Bag 303, Chichiri, Blantyre 3, Malawi
[d] Department of Physics, University of Cape Coast, Ghana
[e] University of the Western Cape, Physics Department, Robert Sobukwe Road, Bellville 7323

ARTICLE INFO

Article history:
Received 30 March 2020
Received in revised form
13 July 2020
Accepted 8 August 2020
Available online 12 August 2020

Keywords:
α-Cr_2O_3
Sweet potatoes peels
XRD
Magnetism
Density functional theory (DFT)

ABSTRACT

A selective single phase black α-Cr_2O_3 nanoparticles was bio-synthesised via simple straight-forward green synthesis approach. The process involves extraction of phytochemicals contained in peels of sweet potatoes. Extraction was done in distilled water under constant magnetic stirring at a temperature of 70–80 °C resulting in a dusty yellow colour aqueous extracts. Afterwards, chromic nitrate salt was added to extracts resulting in reduction of metal salt to metal nanoparticles. Obtained precipitates were dried and annealed in the air for 2 h ready to be applied without further post synthesis modifications. SEM and EDS analysis of annealed precipitates reveal distinct shapes and high purity of nanoparticles. The effects of the annealing temperature are evident in the nanoparticle sizes. SAED and XRD patterns expose bright diffraction peaks which are harmonized to the rhombohedral structure of pure Eskolaiteα-Cr_2O_3. By quantitative analysis of XRD data, it was noted that lattice parameters and crystal sizes slightly decrease w.r.t increase annealing temperature. Raman spectra recorded peaks ascribe to vibrations in A_{1g} and E_g mode whereas FTIR analysis show absorption bands at 641 and 632 cm^{-1} which evidence the presence of α-Cr_2O_3 nanoparticles. UV–Vis absorbance peak generated Cr_2O_3 nanoparticles are observed at 402 nm yielding a band gap of 3.08eV. Magnetism results of α-Cr_2O_3 nanoparticles shows linear increase upon field increasing, which can be elucidated by the existing of uncompensated spins at the surface of the nanoparticles that may lead to nonmagnetic or antiferromagnetic state. Zero field cooling (ZFC) results of α-Cr_2O_3 nanoparticles were analysed based on Curie-Wien relation which yield values of magnetic moment (μ_{eff}) of the synthesised Cr_2O_3 nanoparticles close to the value that was assigned for Cr^{2+}.The density functional theory (DFT) with the PW91, PBE, PBESOL and a Hubbard U Coulomb interactionwas utilized to study the optimum structure, electronic and magnetic properties of antiferromagnetically ordered Cr_2O_3. The computed results are consistent with the experimental measurements.

1. Introduction

Chromium oxide exhibits different phase composition due to thermodynamic properties of its Cr–O binary system. Some reported oxides whose chromium valences are combination of three and six include Cr_3O_8, Cr_5O_{12}, Cr_2O_5, Cr_6O_{15} [1,2]. Of these higher oxides, Cr_2O_3which is an inorganic trivalent oxide widely known for its stability in the Cr–O binary system under ambient conditions has received significant attention [3]. Of particular interests to the scientific community is Cr_2O_3 nanoparticles. Owing to their particle size and shape tenability, Cr_2O_3 nanoparticles with a wide band gap of 3.0eVhave become the centre of attention for robust research and industrial applications.They have found application in coating materials [4], digital recording systems [5], wear resistance [6], pigment [7], colorant [8] as well as in selective solar energy collectors [9].

* Corresponding author. Nanosciences African Network (NANOAFNET), iThemba LABS-National Research Foundation, Old Faure road, 7129, Somerset West, South Africa.
E-mail address: sackey@tlabs.ac.za (J. Sackey).

https://doi.org/10.1016/j.jallcom.2020.156671
0925-8388/

Conventional approach to syntheses nano-sized Cr_2O_3 particle includessolid thermal decomposition [10],hydrothermal process [11] and sol-gel method [12].Kim, Dae-Wook et al. [12] employed precipitation−gelation reaction method and calcined at different temperatures to obtained chromic oxide nanoparticles of different sizes. Zhong, Z. C., et al. [13]used laser induced deposition technique to fabricate nanoscale Cr_2O_3particles. Tsuzuki, and McCormick [14] reported a study on synthesis of Cr_2O_3 nanoparticles via mechanochemicalreaction of sodium dichromate and sulphur. By using gas-condensation method, Balachandran, U.et al. [15]synthesised nanophaseCr_2O_3 with average particles size of 10 nm. In a similar fashion D. Vollath, D. et al. [16]synthesisednanocrystalline Cr_2O_3, particles in microwave plasma.

Yet, the above-mentioned physical and chemical methods have some limitationson usingnano-sized Cr_2O_3particles in industrial applications. This is because, the methods produce low yield, require the use of harmful chemicals, expensive preparation routes and equipment's. Therefore, the R &D community has endorsed bio-synthesismethodor green process which involves the use of microorganism or plants parts to syntheses various nanoparticles including Cr_2O_3 nanoparticles.

Nowadays, bio-synthesis of nanoparticles using plant extractsis popular owing to the fact that the process is cost-effective, eco-friendly, clean, simple, produces high yield, reliable, biocompatible, and offers a better alternative to chemical and physical methods [17]. Nanoparticles synthesised via plant extracts exploit phytochemicalscontained in the plant to operate as reducing agents and singlet oxygen scavengers, therefore reducing metal salts to nanoscale. As such resultant nanoparticles of various sizes, shapes and with better stability can be instantly applied without any post synthesis modification. Furthermore, with abundance plant diversity especially in Africa, research on bio-synthesis of

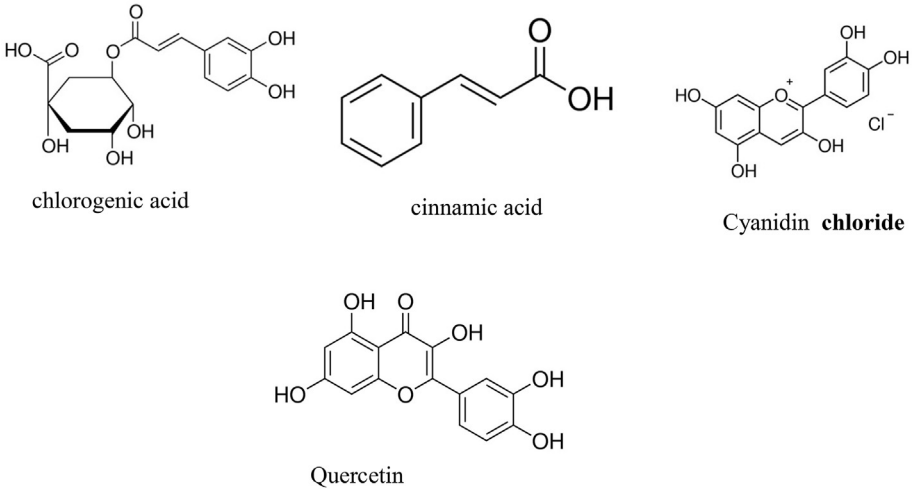

Fig. 1. Phytochemical constituents in sweet potatoes peels.

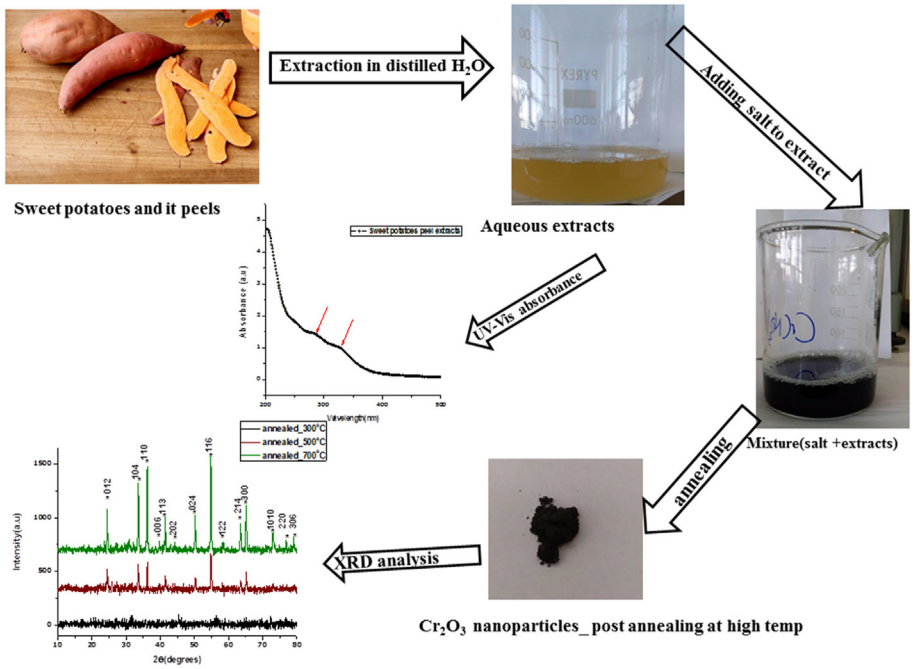

Fig. 2. Graphical diagram of bio-synthesis of Cr_2O_3 nanoparticles using extracts obtained from sweet potatoes peels.

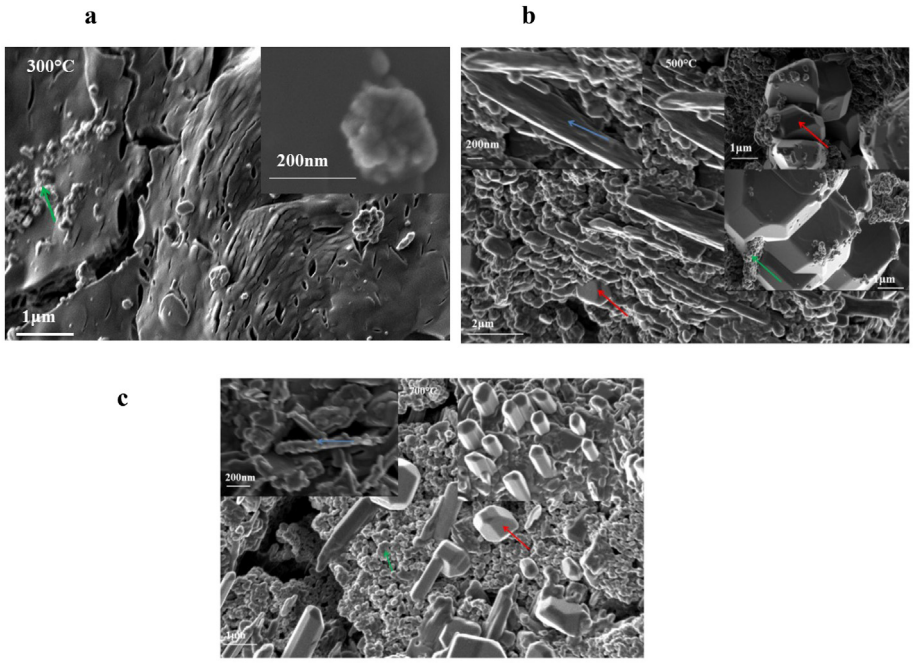

Fig. 3. SEM images of Cr_2O_3nanoparticles showing morphology of samples annealed at (a) 300 °C, (b) 500 °C, (c) 700 °C.

nanoparticles using plant parts such as seeds, fruits, leaves, barks, roots, peels still extensively on-going [18–20]. Discovered abundant plants with bioactive elements used in synthesis of nanoparticles consider as attractive field for researches and scientists. Each plant extracts has unique metabolites responsible for nanoparticles formation. Hence, innovation comes from specific plant or plant parts that are used in the study to achieve a better response compared with other studies.

Sweet potato scientifically known as Ipomoea batatas L. is one of the most important consumed crops in many parts of the world due to its economic and health benefits. It peels are however discarded yet they contain several phytochemical constituents (see Fig. 1) such as phenolic [21], flavonoid, alkaloids, steroids, saponins, tannins and anthocyanin β-carotene [22].Some reported pharmaceutical activities, associated withpeels of sweet potatoes are antioxidant, anticancer activity, antidiabetic activity and anti-inflammatory activity [23].

In view of this, the present study report for the first time biosynthesis of black α Cr2O3 nanoparticles using sweet potatoes peel extracts. The structure, electronic, optical and magnetic properties of chromium oxide were analysed experimentally and theoretically.Especially, by using first-principles calculations based

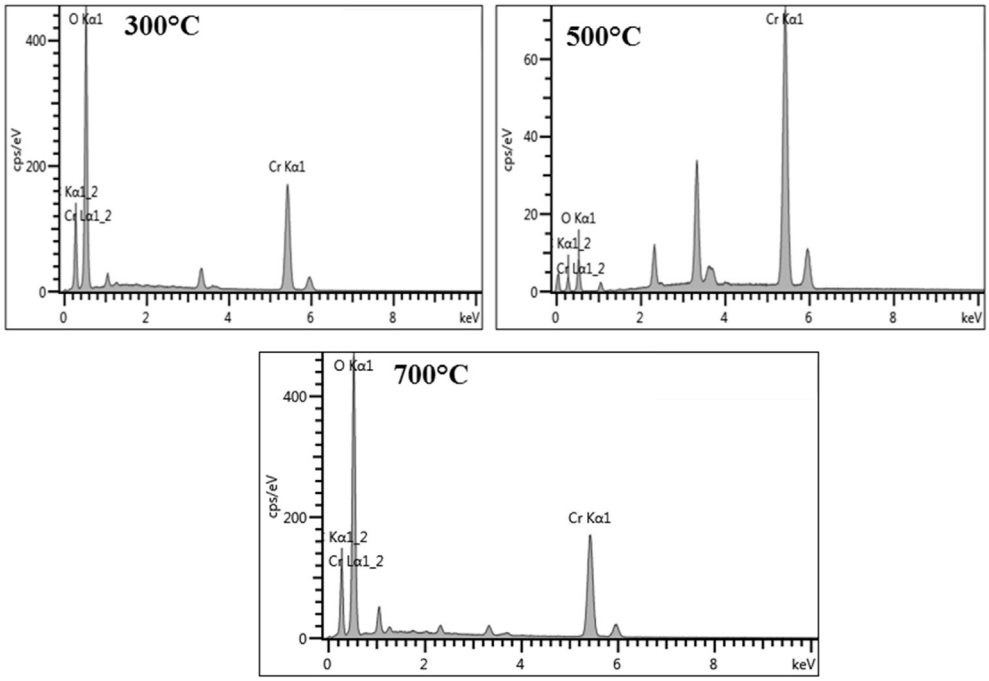

Fig. 4. EDS spectra showing elemental compositions of Cr_2O_3nanoparticles annealed 300°, 500°, 700 °C.

Table 1
Elemental composition of Cr_2O_3 nanoparticles with their respective atomic percentages. Each nanoparticle type and shape reveals different atomic percentages of their elements.

Elements	Atomic % of annealed samples with distinct shapes						
	Atomic % **300°C nanograins**	Atomic % **500°C nanograins**	Atomic % **500°C nanorods**	Atomic % **500°C rhomboid**	Atomic % **700 nanograins**	**Atomic % nanorods**	**Atomic % rhomboid**
O	60.96	7.56	21.99	20.60	61.92	66.22	61.36
Cr	39.04	92.44	78.01	79.40	38.08	33.78	38.64

Table 2
Comparisonof physical properties of Cr_2O_3 nanoparticles using green chemistry approach.

Extracts	Morphology	Particle size (nm)	Band gap (eV)	ref
Mukiamaderspatana	Well separated	65	2.9	[38]
Allium Sativum	Spherical	46–72	3.0	[39]
Callistemon viminalis	Cubic-like	92.2	Didn't report	[40]
Aspargillusniger	Hexagonal	66	2.9	[41]
Tridaxprocumbens	Strips with rough surface	80–100	2.7	[42]
Ipomoea batatas L	rhombohedral, elongated shaped	3, 93	3.08	Present work

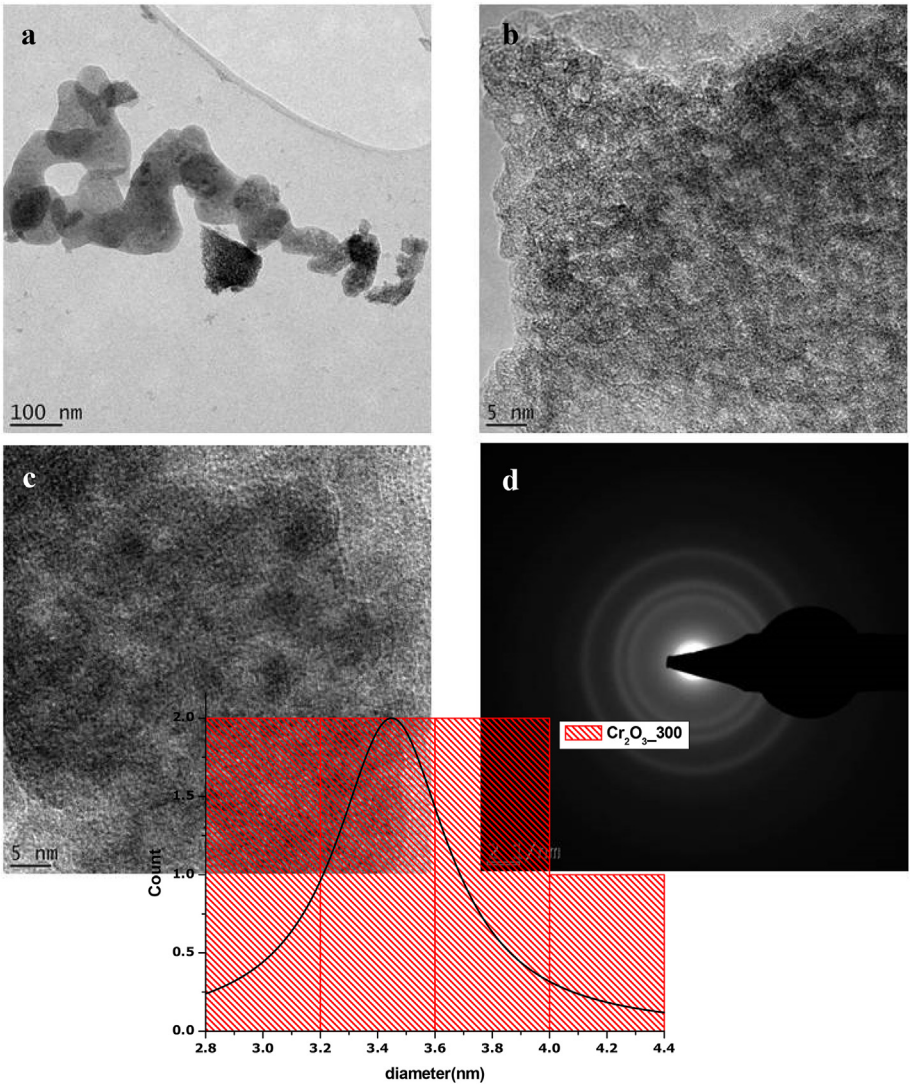

Fig. 5. HRTEM images of Cr_2O_3 nanoparticles annealed at 300 °C showing (a–b) morphology of the nanoparticles, (c) singular nanograin, (d) SAED pattern, inset is the histogram of particle size distribution.

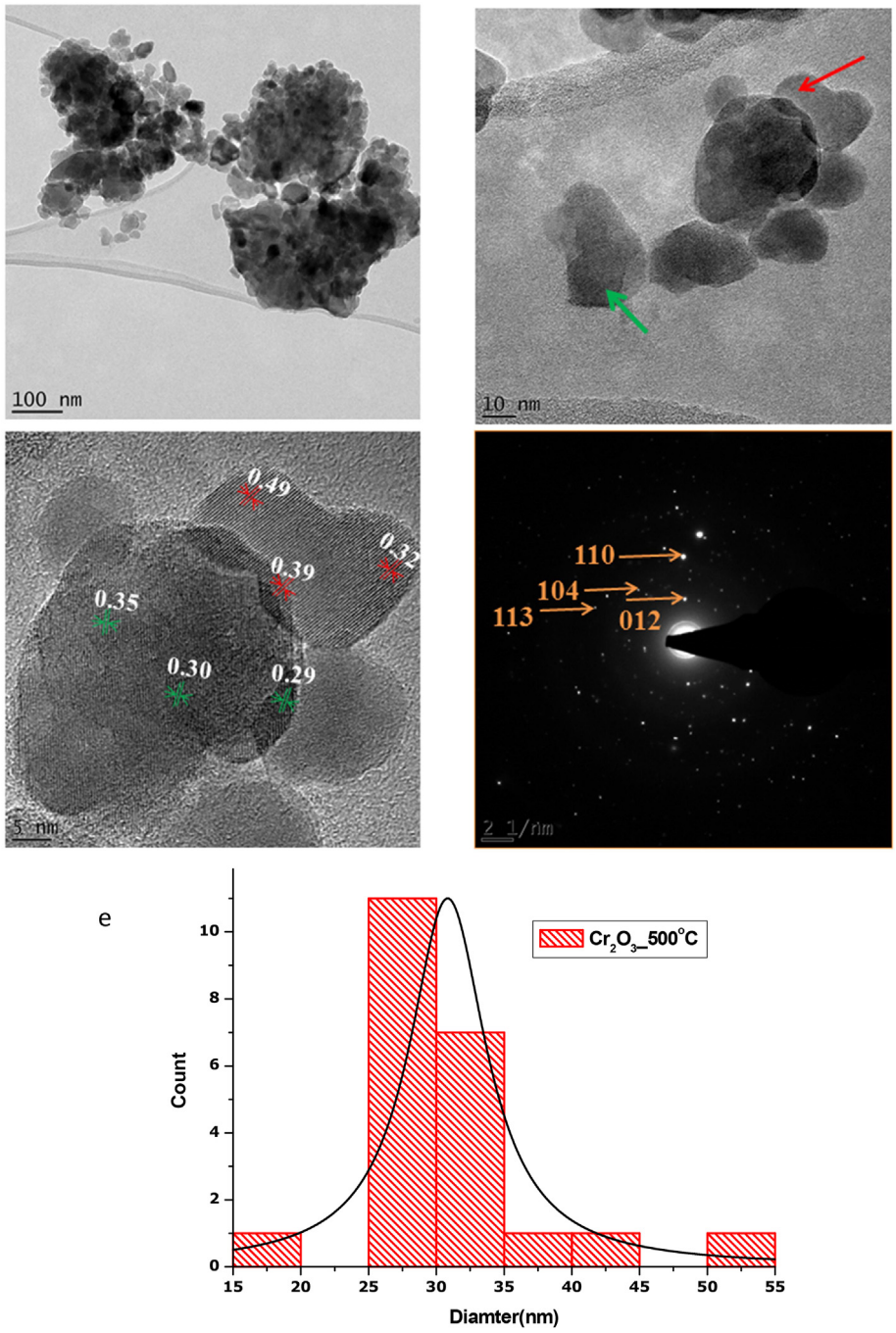

Fig. 6. HRTEM images of Cr_2O_3 nanoparticles annealed at 500 °C showing (a–b) morphology of the nanoparticles, (c) singular nanograin showing distinct planes, (d) SAED pattern, (e) histogram of particle size distribution.

on density functional theory (DFT) within the generalized gradient approximation (GGA), the structural, electronic, and magnetic properties of antiferromagnetic chromium oxide were obtained which are in a good agreement with our experimental investigations.

2. Materials and sample preparation details

Chromicnitrate salt of analytical grade and sweet potatoes were purchased from Hopkin and Williams Ltd and Zimbabwelocal market respectively. For extraction process, peels of sweet potatoes were thoroughly washed several times with distilled water to remove any sand particles and air dried. 100.0g of dried peels were weighed into 300 mL of distilled water. The content was heated at 70–80 °C under constant magnetic stirring for 2 h yieldingdusty yellow colour solution. Obtained aqueous solutionupon cooling was sieved and filtered twice with a laboratory standard test sieve (4 mesh 5 mm aperture) and Whatman filter paper (55 mm cat no 1820055)respectively, to remove any residue. The dusty yellow aqueous extracts ready to be use for synthesis recorded a pH of 7. For bio-synthesis of black α Cr_2O_3nanoparticle using sweet potatoes peel extracts, 2.0g of chromic nitratesalt was added to 50 mL of

previously prepared aqueous extracts resulting immediately to dark blue colour mixture. The pH of the mixture (extracts + salt) dropped to 4. The mixture was allowed to dry at 100 °C in an oven for 9 h and dark blue colour precipitates were collected. The precipitatesobtained post drying were annealed at 300, 500, 700°Cin air for 2 h and subsequently characterized using SEM, EDS, HRTEM, XRD, Raman, FTIR and magnetism. Schematic representation of biosynthesis procedure is illustrated in Fig. 2.

3. Characterization techniques

Annealed samples were carbon coated and imaged by Zeiss crossbeam 540 FEG SEM and high resolution transmission electron microscopy (Tecnai 720). Elemental compositions in the samples were analysed withOxford instrument with a X-max Solid state silicon drift detector.

To identify phase and crystallography of samples, XRD analysis was performed using a Bruker AXS D8 Advance with radiation ($\lambda_{Cuk\alpha}$ = 1.5406 Å).

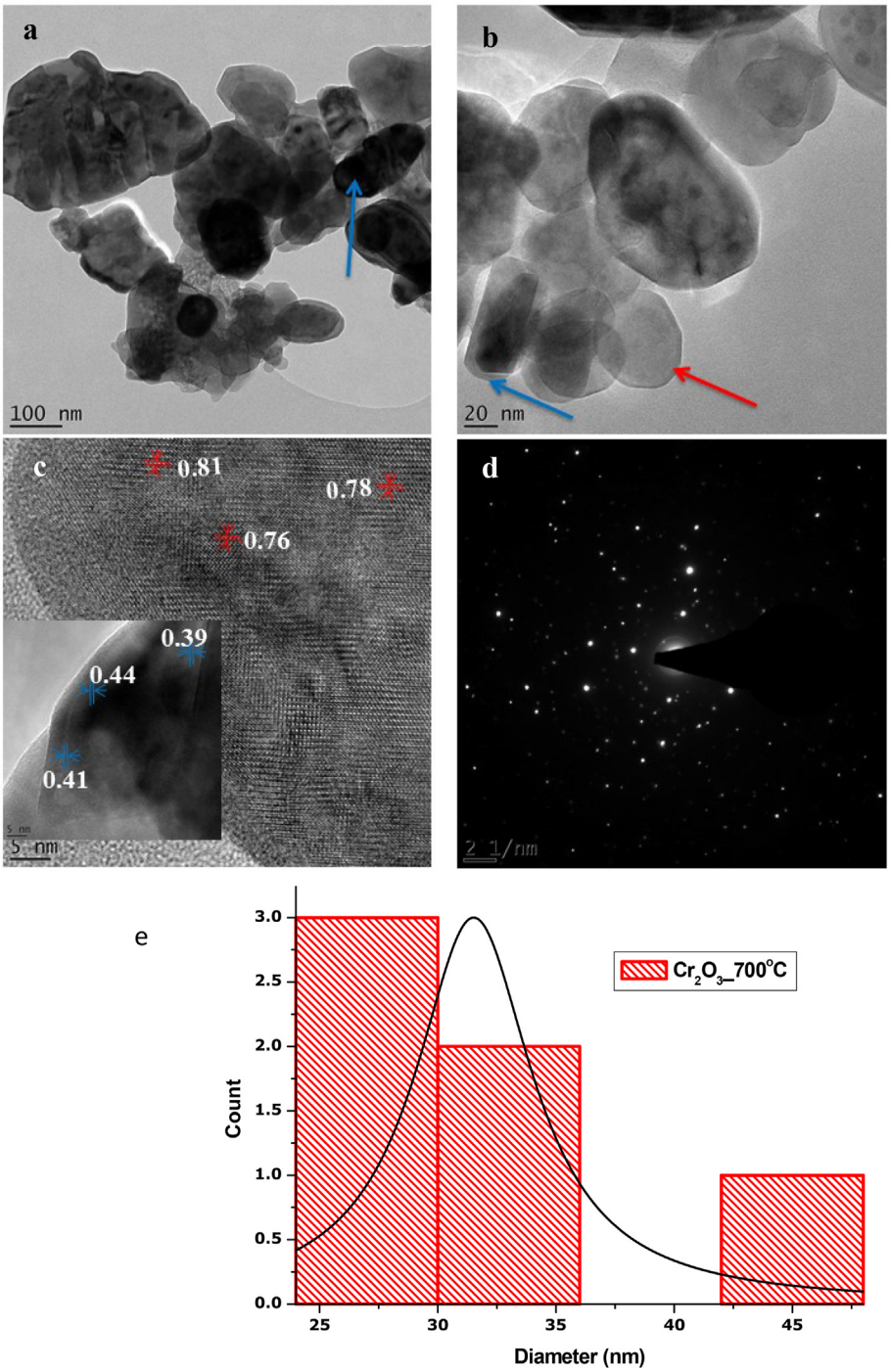

Fig. 7. HRTEM images of Cr_2O_3 nanoparticles annealed at 700 °C showing (a–b) morphology of the nanoparticles, (c) singular nanograin showing distinct planes, (d) SAED pattern, (e) histogram of particle size distribution.

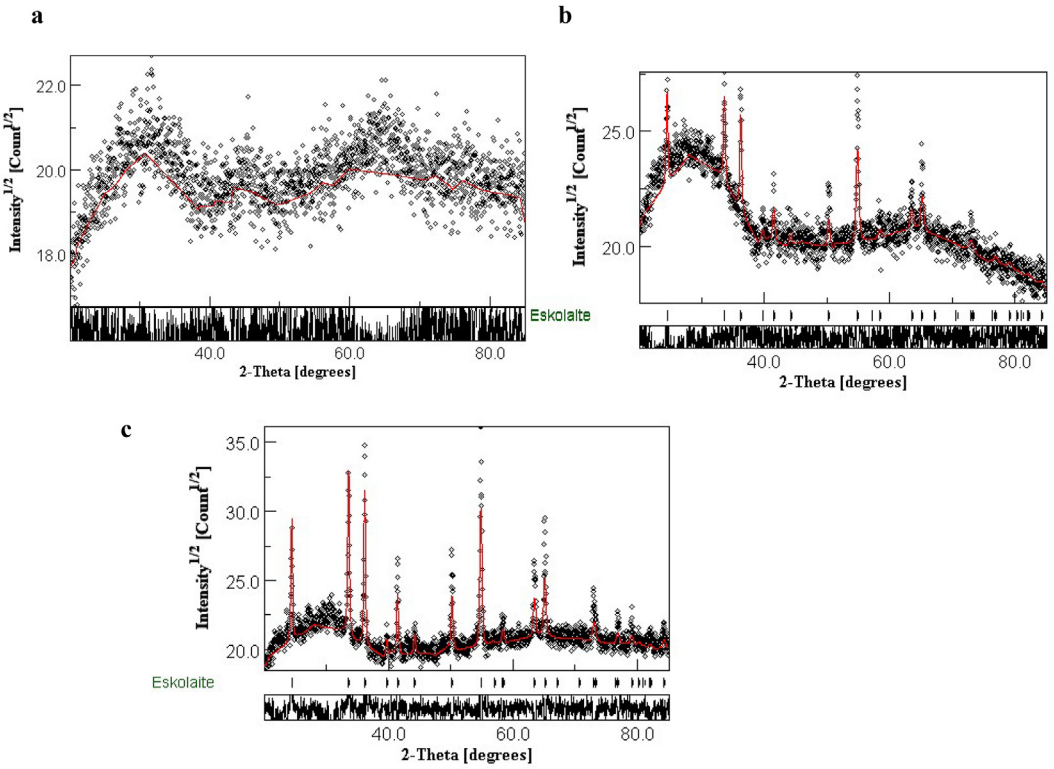

Fig. 8. Observed (black diamond) and calculated (red line) XRD patterns for Cr_2O_3 annealed at (a) 300 °C, (b) 500 °C, (c) 700 °C. (For interpretation of the references to colour in this figure legend, the reader is referred to the Web version of this article.)

Table 3
Refined structure parameters of (a) Cr_2O_3_500°Cand (b) Cr_2O_3_700 °C nanoparticles.

a				
Atom	x	y	z	Biso
Cr	0.000	0.00	0.3423	0
O	0.316	0.00	0.250	0
b				
Atom	x	y	z	Biso
Cr	0.000	0.00	0.3452	0
O	0.327	0.00	0.250	0

A T64000 micro-Raman spectrometer (HORIBA Scientific, JobinYvon Technology) with a 532 nm laser wavelength and spectral acquisition time of 120s was used to investigate the vibrational modes of samples.

To obtain the infrared absorption on samples, we used Fourier-Transform Infrared (FTIR) spectroscopy in the 400−4000 cm^1 range on a PerkinElmer 100 Spectrometer.

UV−Vis absorbance was conducted using Cary 5000 UV−Vis−NIR spectrophotometer with double beam.

A vibrating sample magnetometer (VSM) (Cryogenic ltd, UK) was used to conduct the magnetism study.

4. Computational methods

The density functional theory (DFT) calculations were performed with the Quantum Espresso [24]using the plane-wave basis sets and the Vanderbilt ultra-soft pseudopotentials [25]within the scalar relativistic framework. The structural and electronic properties of the rhombohedral primitive cell of antiferromagnetic Cr_2O_3 were obtained using the spin polarized generalized gradient approximation (GGA) within three different exchange-correlation functionals of PW91 [26], PBE [27] and PBESOL [28].

In order to account the effects of strong intra-atomic electronic correlations, we included a Hubbard U Coulomb interaction [29−34] to the Cr 3d and O 2p states which contribute significantly to the top of the valence band and the bottom of the conduction band. This on-site interaction will increase the energy gap between the occupied and unoccupied states leading to a wider band gap closer to the experimental value.

By applying a range of effective U values between 0 and 8 eV to the Cr d state, the optimized structure, band gap, and magnetic moment of antiferromagnetic Cr_2O_3 are calculated using the PBE functionals. Additionally, the effects of applying the 3 and 5 eV on-site Coulomb interactions to the O 2p states were examined [35].

In the structural optimization a $4 \times 4 \times 4$ k-point mesh over the irreducible Brillouin zone, according to the Monkhorst- Pack scheme [36] was used. For the density of state and the band structure $8 \times 8 \times 8$ k-point grid was employed. A cut-off energy of 650 eV was used for the plane-wave basis set. The convergence threshold for the electronic structure was considered$10^{-6}Ry$.

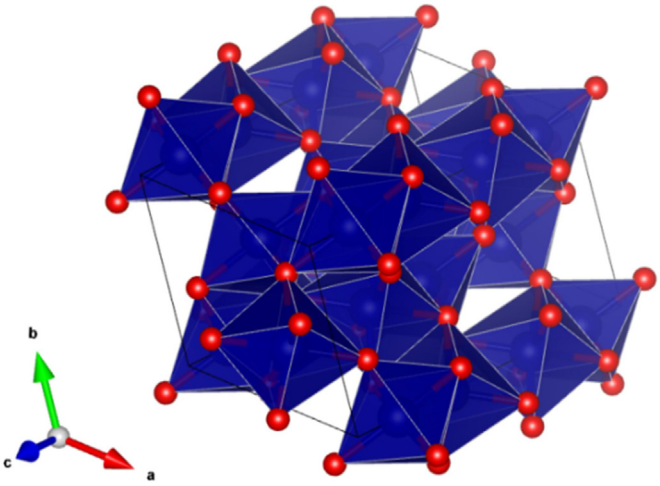

Fig. 9. Unit cell representation of Cr_2O_3 obtained from cell parameters in Table 3.

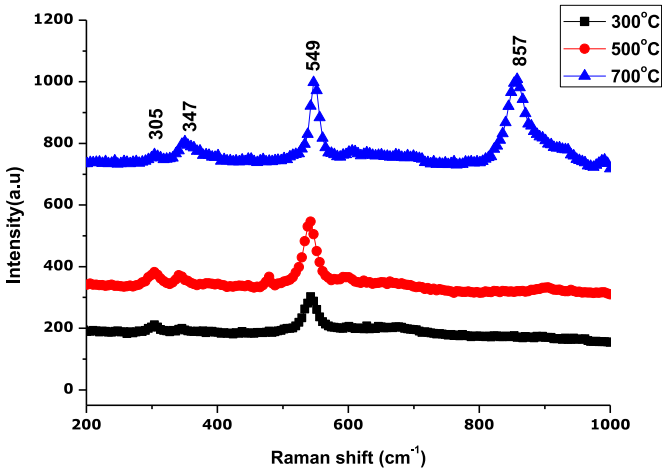

Fig. 10. Raman spectra of Cr_2O_3 nanoparticles annealed at 300 °C, 500 °C, 700 °C.

5. Results and discussion

5.1. Mechanism of nanoparticle formation

Phenolic and Flavonoids are among the active phytochemicals contained in sweet potatoes peels which would act as both chelating and capping agents that result in formation of nanoscale of the particle. For a plausible mechanism of reaction of transformation of chromium nitrate to Cr_2O_3 nanoparticle, a chemical reaction of biological compounds from our plant extracts is proposed. The altered chemical behaviour of active phytochemicals and chromium nitrate may result in oxidation of biological compound through free radical and then followed by electrostatic attraction between free radical and cation of precursors (chromium nitrate). After the heat treatment the product decomposes to give rise to Cr_2O_3 nanoparticles.In accordance with UV–Vis analysis of sweet potatoes peel extracts, two characteristic peaks are observed at 280 and 330 nm associated with absorption due respectively to B-ring cinnamoylsystem and A-ring benzoyl system of flavonoid. In addition, XRD patterns of annealed precipitate exposed Bragg peaks which are perfectly matched to Eskolaiteα-Cr_2O_3nanoparticles. Therefore, it can be inferred that aqueous extracts of sweet potatoes peels which is pH sensitive favours formation of single phase Cr_2O_3nanoparticles.

5.2. SEM,EDS, HRTEM

The morphology of bio-synthesised samples annealed at different temperatures (300 °C, 500 °C, 700 °C)is shown in SEM and HRTEM images. Precisely, Fig. 3 (a,b,c) shows SEM image of Cr_2O_3_300 °C, Cr_2O_3_500 °C andCr_2O_3_700 °Cnanoparticles respectively. It can be seen from SEM image that Cr_2O_3_300 °C nanoparticles are agglomerated and not well formed. One is unable to tell exact shape of nanoparticles. Yet as annealing temperature increased to 500 and 700 °C, (see Fig. 3 (b, c)), one can vividly see well defined nanoparticles with distinguish shapes. Specifically, SEM image for Cr_2O_3_500 °C reveal distinguishable rhomboid shaped nanoparticles (designated by red arrowed), elongated nanorods (blue arrowed) and highly agglomeratednanoparticles (green arrowed). As the temperature increased further to 700 °C, we observed that the agglomerated nanoparticles elongateto form nanorods (See Fig. 3(c)).

From the SEM images only, it can be understood that low annealing temperatures of 300 °C, Cr_2O_3 precipitates undergo incomplete/insufficient oxidation to form well defined nanoparticles. However at higher annealing temperatures of 500 and 700 °C, Cr_2O_3 nanoparticles become well-formed revelling distinct shapes.

To identify chemical elements and purity of synthesised samples, EDS analysis were performed and results are shown in Fig. 4. According to EDS spectra, the most pronounced and only chemical elements presents on samples are O and Cr. Cleary, there are no other chemical elements identified in the sample which confirm purity of synthesised sample as Cr_2O_3nanoparticles.Table 1 gives the atomic percentages of chemical elements on samples. As one can see in this table, there are differences in the atomic percentages of the chemical elements in the different shape of nanoparticles (see Table 2).

HRTEM images of Cr_2O_3_300 °C, nanoparticlesare shown in Fig. 5(a–d). At such annealing temperature of 300 °C, one could observe spiralshaped and agglomerated nanoparticles with average particle size calculated as 3.44 nm (see Fig. 3(a and b)). The singular nanograin shown in Fig. 5(c) is amorphous; hence it is difficult to evaluate the appropriate d_{hkl} distances. Moreover, SAED image displayed in Fig. 5 (d) show rings with no diffraction peaks. The Histogram of particle size distribution of Cr_2O_3_300 °C is shown in inset.

Fig. 6(a–d) shows HRTEM images of Cr_2O_3_500 °C nanoparticles. As can be seen in Fig. 6(a), Cr_2O_3_500 °C is composed of different shapes of nanoparticles with particle diameter ranging from 17 to 50 nm.A singular nanograin shown in Fig. 6(b) reveals distinct shapes designated by red and blue arrows. Each nanograin as displayed in Fig. 6(c) exposes distinguishable planes with appropriate d_{hkl}distance. SAED image shown in Fig. 6(d) exposesbright scattered diffraction spots due to planes which are in harmonized with rhombohedra structure of Eskolaite Cr_2O_3. Histogram of particle size distribution of Cr_2O_3_500 °C is shown in Fig. 6(e).

Table 4
Refined parameters extracted from Rietveld analysis using MAUD. Values presented in parenthesis are calculated uncertainties.

Cr_2O_3 annealed at	a(Å)	c(Å)	Strain ϵ(*1e^4)	Size (Å)
300 °C	–	–	–	–
500 °C	4.95 (10)	13.591 (3)	1.01 (4)	776 (6)
700 °C	4.959 (4)	13.610 (4)	3.590 (5)	924 (9)

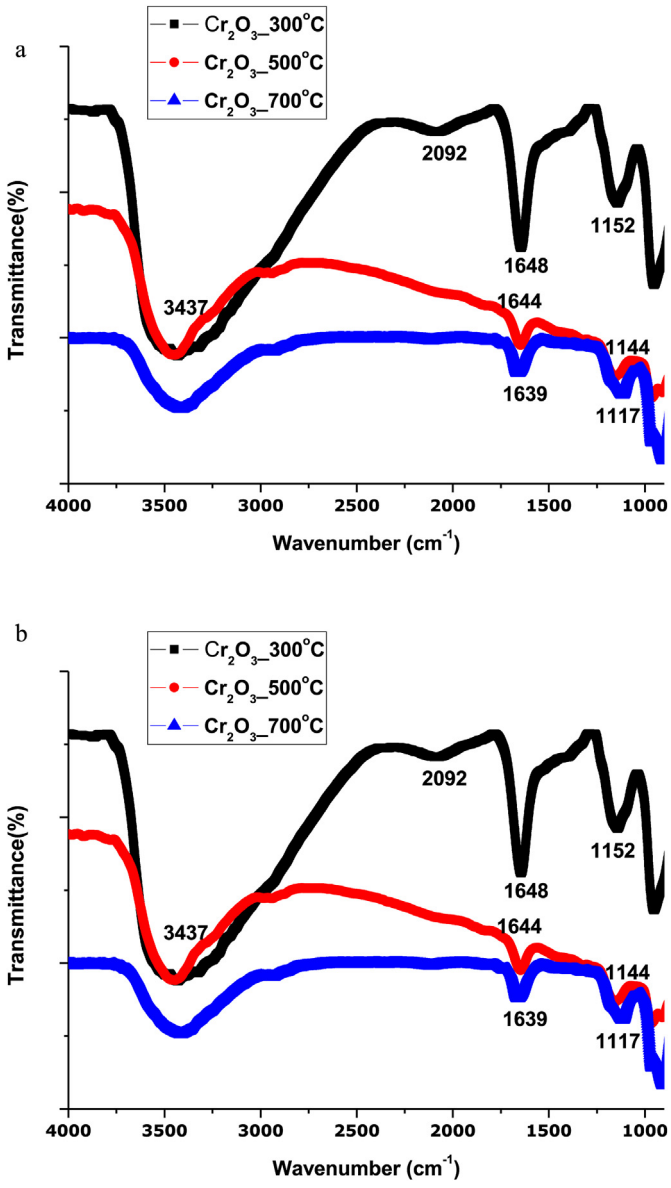

Fig. 11. (a–b): FTIR spectra of annealed Cr_2O_3 nanoparticles at (a) higher wave number, (b) lower wave number.

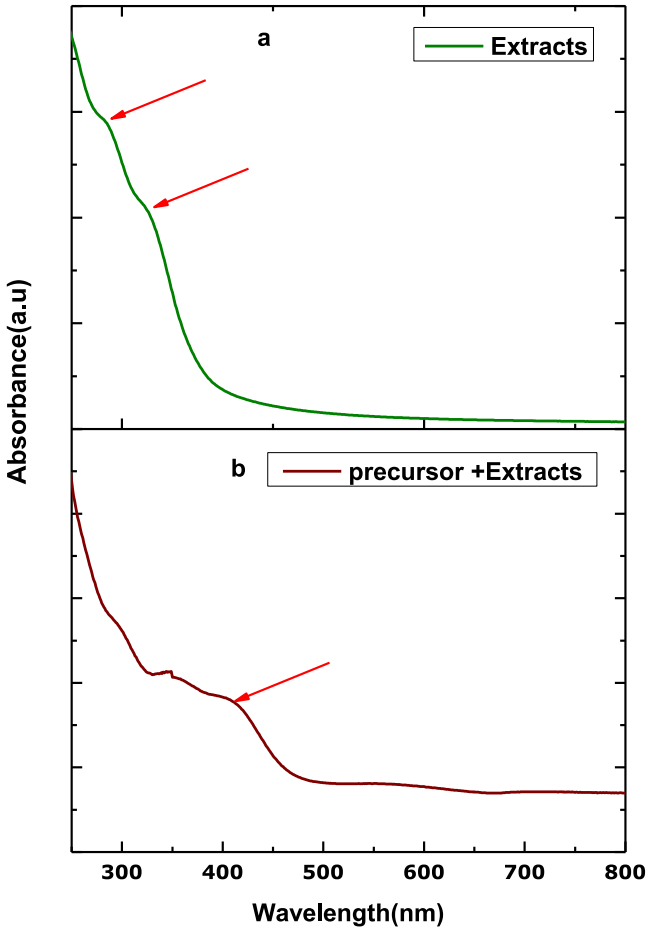

Fig. 12. UV–Vis absorbance spectrum for (a) aqueous sweet potatoes peel extracts, (b) precursor and extracts.

Fig. 7(a–d) present HRTEM images of Cr_2O_3_700 °C which reveal (a,b) elongated nanorods, and rhombohedral shaped nanoparticle designated by blue and red arrow respectively. Average particle size evaluated using image J software is 93.5 nm. Distinct planes with appropriate d_{hkl} distances evaluated as 0.81 nm, 0.78 nm, 0.76 nm and 0.29 nm, 0.44 nm, 0.41 nm on rhombohedra shaped nanoparticles and elongated nanorods respectively are observed on a singular nanograin (See Fig. 7(c)). Fig. 7(d) is SAED image of Cr_2O_3_700 °C which reveals many bright scattered diffraction spots. The presence of so many diffraction spots confirms crystallinity of the samples. Histogram of particle size distribution of Cr_2O_3_700 °C is respectively plotted in Fig. 7(e).

From HRTEM analysis, it is seen that Cr_2O_3_300 °C present almost non-identifiable shape of agglomerated nanoparticles. The corresponding SAED image shows diffuse rings with absence of diffraction peaks. This could indicate amorphous nature of the nanoparticles. In contrary to that, HRTEM images of Cr_2O_3_500 °C reveal well defined shapes of nanoparticles. It is also observed that as annealing temperature is increased further to 700 °C, HRTEM images show presence of well-formednanorods. In addition, the nanoparticle size of Cr_2O_3_700 °C increases. This follows from that fact that particles sizes increases with increasing annealing temperature as it was reported in literature [37]. As evidenced from SAED images of both Cr_2O_3_500 °C and Cr_2O_3_700 °C nanoparticles, so many bright diffraction spot are seen. This confirms the crystalline and poly crystalline nature of Cr_2O_3_500 °C and Cr_2O_3_700 °C nanoparticles respectively.

5.3. Quantitative XRD data analysis using MAUD

Fig. 8 (a,b,c)shows observed and calculated crystallographic phase of synthesised annealed samples investigated by XRD spectroscopy and MAUD analysis. Materials Analysis Using Diffraction (MAUD) software is a Rietveld program which was used to fit the XRD diffraction data [43]. It is observed from XRD pattern that samples annealed at 300 °C show no peaks. This means, at lower annealing temperature, nanoparticles are amorphous. Nonetheless at higher annealing temperature (500, 700 °C), XRD spectra shows series of peaks with increase intensity w.r.t increased annealing temperature. MAUD software was used to quantitatively analyze the XRD patterns and retrieve relevant information such as lattice parameters, strain, size and atomic positions. Atomic positions are reported in Table 3 with the cell representation shows at Fig. 9.

Rhombohedral structure proposed by Kantor, Anastasia, et al. [44]of Eskolaite Cr_2O_3which belong to R-3cH space group was used

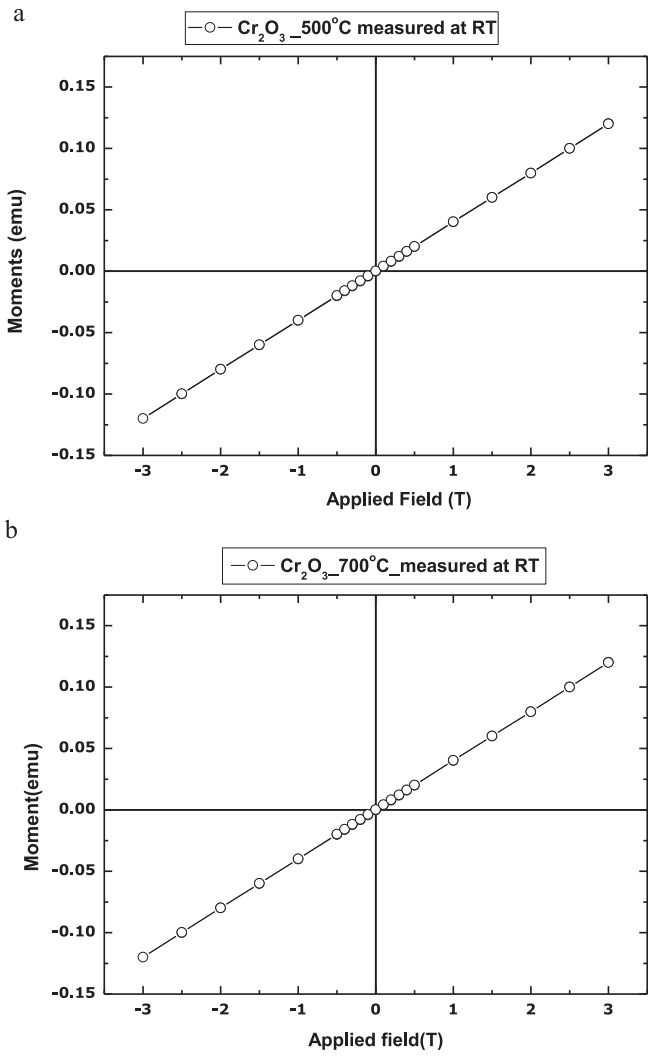

Fig. 13. Field-dependent magnetization measured at room temperature (Rt) for (a) Cr2O3_500 °C and (b) Cr2O3_700 °C.

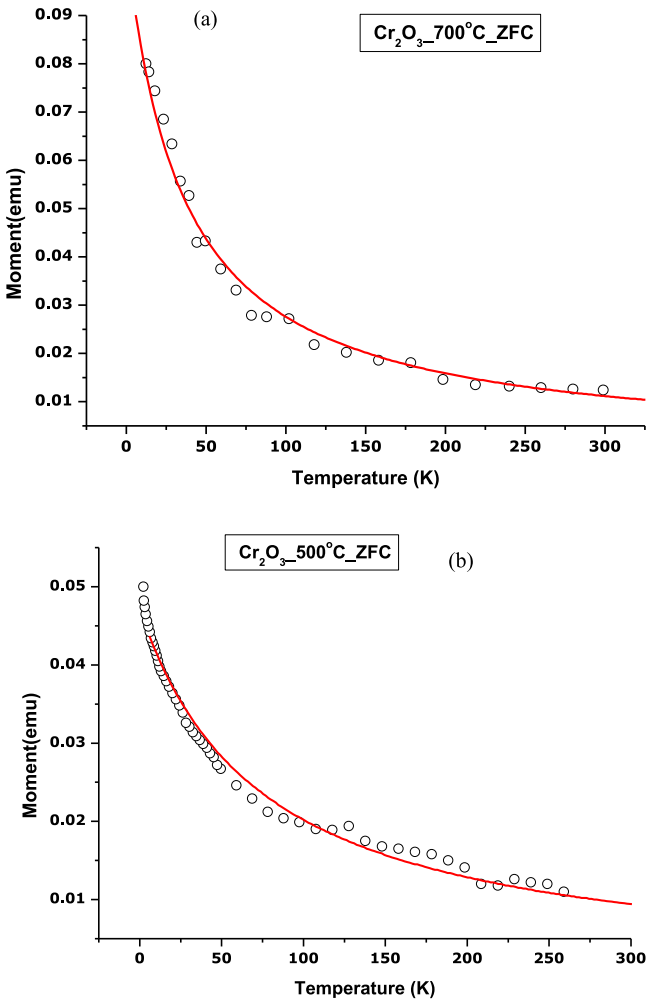

Fig. 14. Zero - field cooling (ZFC) results between 2 K and 300 K for (a) Cr2O3_500 °C and (b) Cr2O3_700 °C nanoparticles. Black open circles represent experimental date while red solid lines represent the least square fitting (LSQ) of ZFC data. (For interpretation of the references to colour in this figure legend, the reader is referred to the Web version of this article.)

to fit experimental data. As can be seen, the model fit fairly well with experimental data. From Rietveld analysis, lattice parameters of Cr_2O_3nanoparticles w.r.t annealing temperature were evaluated. Accordingly, lattice parameters (a, c) decreases slightly for samples of lower annealing temperature (See Table 4).

From quantitative XRDanalysis, it can be deduced that crystallite size increases with increasing annealing temperature. This observation is in agreement with conclusions obtained from SEM and HRTEM analysis.

5.4. Raman, FTIR

In order to determinevibrational mode of the synthesised annealed samples, Raman spectroscopy at ambient conditions was performed. A laser source of 532 nm was used to excite the samples and results are shown in Fig. 10. According to reports obtained from literature, Raman spectra for Cr_2O_3 nanoparticles record about five to six peaks [45]. Though other researchers report more than six Raman peaks from Cr_2O_3 nanoparticles. For instance, Hart, T.R. et al. [46]reported seven Raman peaks of Cr_2O_3synthetized at ambient conditions. They assigned two A_1g modes of Cr_2O_3 at 266 and 547 cm^{-1}, and five E_g modes at 235, 290, 352, 528 and 617 cm^{-1}. McCarty, K. F. and Boehme, D. R [47].reported six Raman bands and identified the bands centred at 304 cm^{-1} and 553 cm^{-1} as A_1g summery and other bands centred at 353, 401, 529, 616 cm^{-1} as $E_g$symmetry of chromium oxide.Shim, Sang-Heon et al. [48] observed a Raman shift (556 cm^{-1}) of Cr_2O_3 measured at 0.09 GPa.

In the present work, Ramaninvestigation of sweet potatoes peel mediated Cr_2O_3nanoparticles, recordedfourRaman peaks. The Raman spectra shown in Fig.10present one distinguishable peak identical on all annealed samples. This peak is centred at 547 cm^{-1} and is ascribed to the A_1g modes.In addition, other less intense peaks at 305 and 347 cm^{-1} ascribe to vibrations in A_1g and $E_g$modes respectively are identified in the samples. These peaks are consistent with the peaks of Cr_2O_3which have been reported in literature [49,50]. It is also seen that at higher annealing temperature of 700 °C, additional peak is observed at 857 cm^{-1} which could be assigned to the Cr^{VI}–O vibrations of symmetric phonon modes. Yang, Jing, et al. [51]reporteda similar peak on synthetic chromium oxide gel investigated using hot-stage Raman spectroscopy. They attributed the peak to the symmetric stretching modes of $O–Cr^{III}–OH$. All the peaks observed from the Raman spectra on our sample correspond to chromium oxide.

Fig. 11 (a-b)present FTIR spectra ofsweet potatoes peel mediated Cr_2O_3 nanoparticles.The spectra show shifts in wave numbers of

absorption with increasing annealing temperature. More accurately, one can noticechanges incharacteristics peaks which become shaper with increasing annealing temperature. This could be an indicative of crystallinity of annealed samples. On the FTIR spectra (Fig. 11 (a)), N–H stretching observed at 3437 cm^{-1} is identified on all samples. However, stretching vibrations of C–H observed at 2092 cm^{-1} is identified on only Cr_2O_3_300 °C. In addition, C=O stretching vibration are identified on all samples though observed at different wave numbers. For instance, one can see absorption at 1648, 1644, 1639 cm^{-1} (see Fig. 11(a)) corresponding to C=O stretching in Cr_2O_3_300 °C, Cr_2O_3_500 °C, Cr_2O_3_700 °C respectively. Meanwhile, absorption bands observed at 1152, 1144, 1117 cm^{-1} which is assigned to C–N vibration is identified on Cr_2O_3_300 °C, Cr_2O_3_500 °C, Cr_2O_3_700 °C respectively. The peaks at 951, 907 and 903 cm^{-1} (see Fig. 11(b)) are assigned to the Cr=O vibrations [52]. One can also see absorption bands at 641 and 632 cm^{-1}which are evidence of the presence of α-Cr_2O_3nanoparticle. At lower wave numbers (Fig. 11(b)) such as 584, 578, 574 cm^{-1}, other absorption bandswhich are typical of O–Cr–O vibrations are observed. These bands are attributed to the $E_u$mode. Such bands are similar to what has been reported in literature for Cr_2O_3 [40].

5.5. Optical analysis

To identify the phytochemicals responsible for reducing metals salt to its nanoscale and to determine the band gap for the samples, UV–Vis absorbance was measured. Fig. 12 (a) shows UV–Vis absorbance spectrum for freshly prepared sweet potatoes peels extracts. Two strong absorbance peaks are seen at 285 and 330 nm. These prominent peaks are indicative of the presence of phenolicand flavonoids [53]. As stated in the introduction, phenolicand flavonoid are identified in Ipomoea batatas L. and thus considered as reducing agents in synthesis of Cr_2O_3 nanoparticles.

Fig. 12(b) shows absorbance spectrum of mixture (precursor + extracts). It should be noted that measurement was recorded immediately precursor was added to extracts. Therefore immediate appearance of peak suggests instant nanoparticle

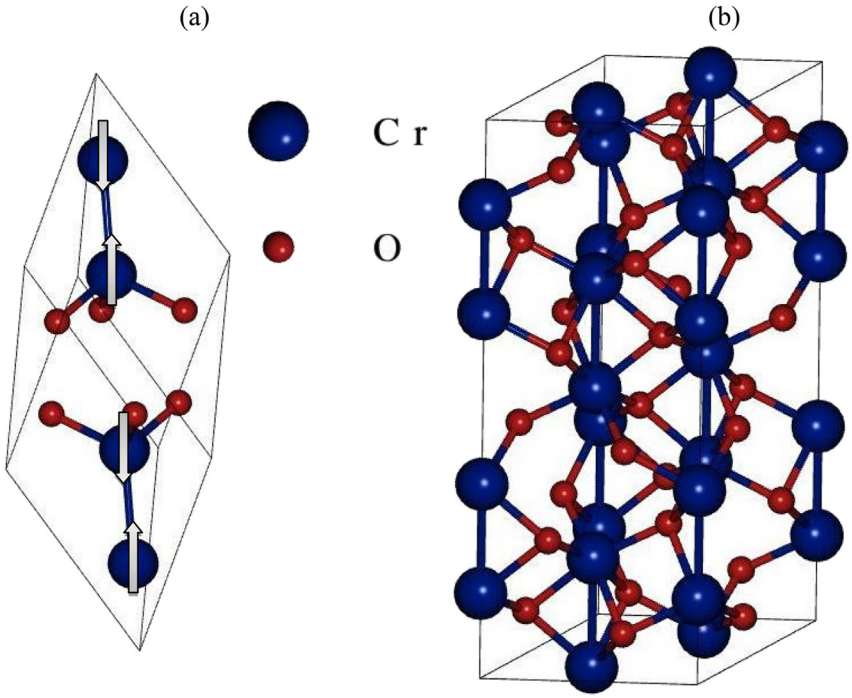

Fig. 15. (a) Rhombohedral primitive cell of Cr_2O_3 with antiferromagnetic spin order (b) Hexagonal Unitcell of Cr_2O_3.

Table 5
Lattice constants a and c, axial ratio c/a, magnetic moment (μ_B), and band gap E_g of antiferromagnetic Cr_2O_3. Our results are compatible with the other DFT calculations based on DFT + U. In Ref. [59]the effective U–J = 4 eV.

Functional			$a\ [A^o]$	$c\ [A^o]$	c/a	$\mu\ [\mu_B/atom]$	$E_g\ [eV]$
PW91			4.937	13.818	2.798	2.021	1.580
PBESOL			4.845	13.762	2.840	2.121	1.540
PBE + D3			4.917	13.792	2.806	2.218	1.560
PBE + U	$U_{Cr}[eV]$	U_O [eV]					
	3	0	5.028	13.775	2.74	2.56	2.415
	3	3	5.015	13.714	2.73	2.482	2.798
	3	5	5.007	13.697	2.74	2.483	2.928
	6	0	5.102	13.862	2.72	2.612	2.882
	6	3	5.082	13.819	2.72	2.585	3.357
PBE + U [32]	3	5	5.028	13.794	2.74	–	2.96
PBE + U [58]	4*	0	5.073	13.839	2.727	3.01	2.6
Exp (This work)			4.959	13.610	2.74	2.48 [58]	3.080

formation. Proposed mechanism of reaction is based on chemical reaction between flavonoids in extracts andchromic nitrate salt giving rise to Cr_2O_3 nanoparticles. The absorbance peakgenerated Cr_2O_3nanoparticles isnoted at 402 nm. Energy Band gap energy was estimated by using Planck's equation given as;

$$E_g = \frac{hc}{\lambda} \quad (1)$$

Where*h*is Planck'sconstant, *c*is speed of light, $\lambda$is the wavelength, $E_g$is the band gap energy. From equation (1), estimates energy band gap is 3.08eV which is consistent with value reported in literature for Cr_2O_3nanoparticles.

5.6. Magnetism study

To further investigate the physical properties of the synthesised nanoparticles, we have performed the magnetic measurements on two samples, i.e, Cr_2O_3_500 °C and Cr_2O_3_700 °C nanoparticles using the vibrating-sample magnetometer (VSM).The field-dependent magnetization measured at room temperature (R_t) are shown in Fig. 13(a) and (b) for Cr_2O_3_500 °C and Cr_2O_3_700 °C nanoparticles, respectively. To obtain accurate results, these measurements were performed on a small portion of the powder that was inserted into a capsule and packed with small amount of vacuum grease to avoid gross motion of the powder in the magnetic field. It is clear from Fig. 13(a) and (b) that magnetization results of all samples show a linear increase upon field increasing. Such linear behaviour followed from the fact thatCr_2O_3 nanoparticles annealed at different temperatures possess unsaturated moments that would result in a linear, paramagnetic contribution to the magnetization.Moreover, this behaviour can beelucidated by the existing of uncompensated spins at the surface of Cr_2O_3 nanoparticleswhich may lead to nonmagnetic or antiferromagnetic state of the nanoparticles as it was evident from literature [54,55].

In order to confirm the magnetic and oxidation stateof the synthesised nanoparticles, we have presented Zero - field cooling (ZFC) results between 2 K and 300 K for Cr_2O_3_500 °C and Cr_2O_3_700 °C nanoparticles in Fig. 14(a) and b, respectively. Asitcan be seen from the (ZFC) results of the two samples that the magnetic moments increases upon cooling and no evident of any kind of magnetic orderingoccurring in the measured temperatures range.Thusthe enhanced magnetic moments may originate from the uncompensated spins at the surfaceof the synthesised Cr_2O_3nanoparticles or due to the variance between the inner and internal spins of the surface of Cr atoms [56]. However, (ZFC) data could be fitted to Curie-Wien relation [51,52] given as

$$\chi = \frac{N_A\,\mu_{eff}^2}{3k_B\,(T-\theta_P)} \quad (2)$$

where $\chi$is the magnetic susceptibility, N_A is Avogadro's number, K_B is Boltzmann's constant, μ_{eff} is effective magnetic moment and θp is curie temperature. The least square fitting (LSQ) of (ZFC) data of Cr_2O_3_500 °C and Cr_2O_3_700 °C nanoparticles to Curie-Wien relation are shown by red solid line Fig. 14(a) and b. The values of μ_{eff} obtained from (LSQ) are 5.23 BM and 5.07 BM for Cr_2O_3_500 °C and Cr_2O_3_700 °C nanoparticles, respectively. It should be noted that the obtained values ofμ_{eff} are much close to that value of 4.9BM assigned for Cr^{2+} ion [53].Therefore based on the values of $\mu_{eff}$of the synthesised Cr_2O_3nanoparticles, one can expect that the surface of Cr ion is Cr^{2+} rather than Cr^{3+}. On the other hand, the values of θp obtained from the (LSQ) are −55.32 and −72.85 for Cr_2O_3_500 °C and Cr_2O_3_700 °C nanoparticles, respectively. It is noted from the literature [56,57]that the negative values of θp are assigned for the antiferromagnetic materials. Thus thevalues of θp may indicate that the synthesised Cr_2O_3 nanoparticles are mostly antiferromagnetic.

5.7. Structural, electronic and magnetic propertiesfrom DFT analysis

Cr_2O_3 can be described by a rhombohedra unit cellor hexagonal cell parameterswith$R\bar{3}c$ space group represented in Fig. 15(a) and (b), respectively. It is antiferromagnetic in the ground state with a (+- + -) spins for the Cr atoms along the c-axis [31,33].

The geometry of antiferromagnetic rhombohedral unit cell of

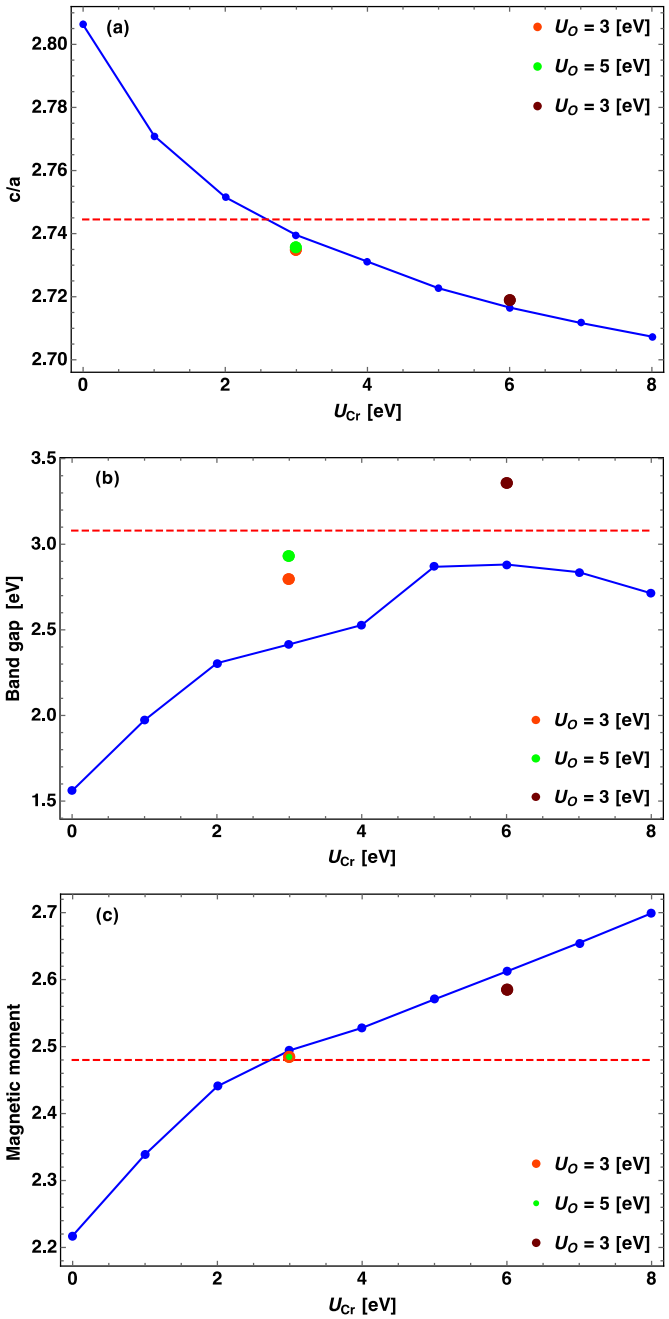

Fig. 16. (a) The ratio of cell-lengths c/a in Hexagonal cell (b) the band gap and (c) the magnetic moment for Cr_2O_3 versus U_{Cr} (eV). The red, green and dark red points represent the results after applying the U potential to the O orbitals. (For interpretation of the references to colour in this figure legend, the reader is referred to the Web version of this article.)

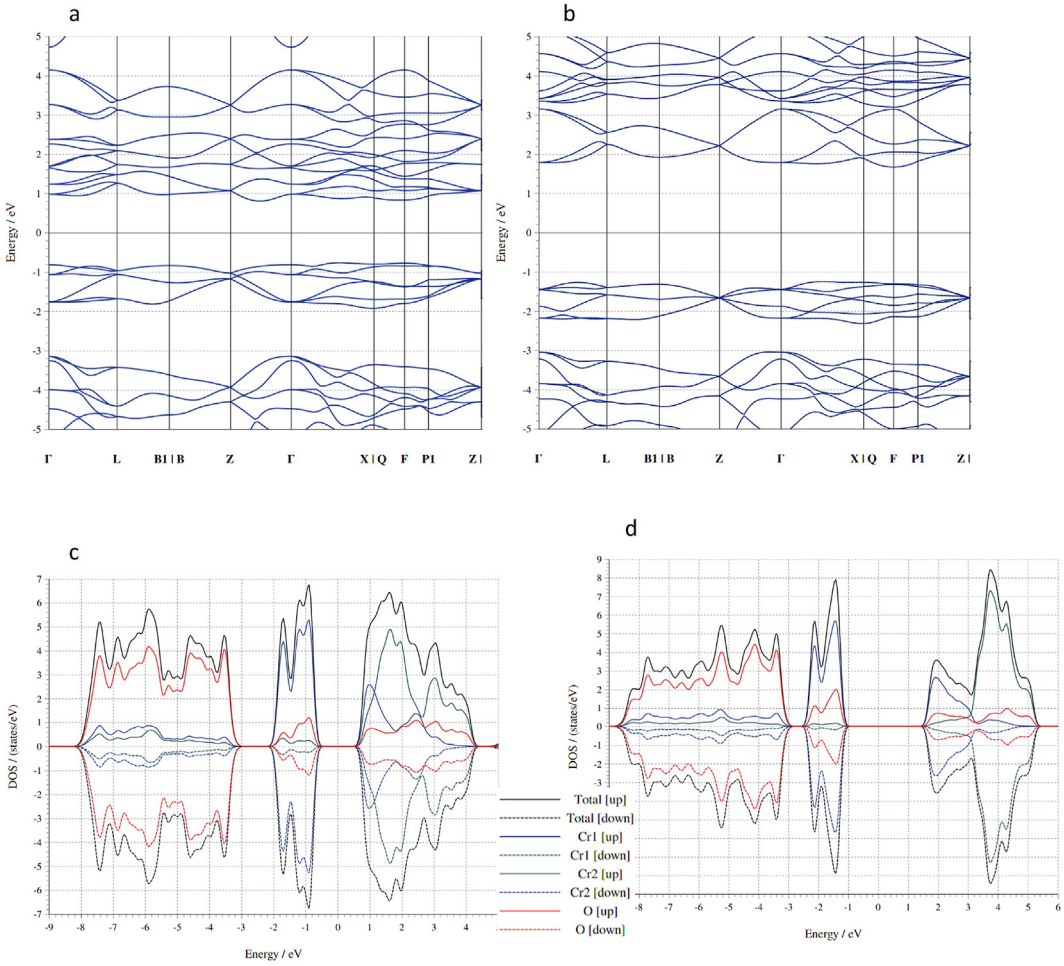

Fig. 17. The band structure of anti-ferromagnetic Cr_2O_3 using (a) PBE functional (b) after applying $U_{Cr} = 3, U_O = 5\ eV$. Electronic total and partial density of states of bulk Cr_2O_3calculated with (c) PBE functional (d) after applying $U_{Cr} = 3, U_O = 5\ eV$.

chromia was optimized using the PW91, PBE, and PBESOL. The calculated lattice constants, magnetic moments, and band gap are listed in Table 5. Generally, PW91, PBESOL and PBE functionals overestimate the ratio of lattice constants by 1.9%, 3.5%, and 2.3%, respectively and underestimate the band gap and the magnetic moment.

For the PBE + D3 calculations, we applied the Hubbard potential to the Cr atoms in the range 1−8 eV. The ratio of lattice constants, band gap and magnetic moment versus the $U_{Cr}$are plotted in Fig. 16. The structural ratio and the magnetic moment match with our experimental value for $U_{Cr} = 2.5\ eV$ roughly, while the band gap is still much lower than the observed one. By increasing the U parameter, the structural ratio decreases, while the band gap and magnetic moment increase. GGA + U with $U_{Cr} = 6.0\ eV$ give rises to the largest band gap of 2.88 eV.

In order to correctly model the valence band, it is required to apply a +U to the O p states in addition to the Cr d states [32,33]. Here, we examined a few values of a +U applied to the O p state. Results illustrated with the filled circles in Fig. 16 indicate that the chosen values of $U_{Cr} = 3\ eV$ and $U_O = 5\ eV$ overestimate the values of a and c by 0.048 and 0.087 A, respectively. The magnetic moment overestimate just by 0.01% and the band gap underestimate by 5% compared to our experiment.

Fig. 17 shows the band structures, total and partial electronic density of states of antiferromagnetic Cr_2O_3 calculated with the PBE, PBE + U ($U_{Cr} = 3$ eVand $U_O = 5\ eV$). Applying the U interaction increases the indirect band gap from 1.560 to 2.9 eV which is very close to the value observed in our experiments.

Generally, the values of $U_{Cr} = 3, U_O = 5\ eV$ leads to an acceptable agreement between the structural and the electronic properties with our experiment.

6. Conclusion

The study reports experimental and computation analysis of bio-synthesised black α-Cr_2O_3 nanoparticles. Aqueous extracts obtained from peels of sweet potatoes serve as reducing agents in bio-synthesis approach. SEM analysis of annealed samples reveals rhomboid shapenanoparticles and elongated nanorodswhile EDS analysis confirmed synthesise of pureCr_2O_3 devoid of any impurity. HRTEM images reveal singular nanograins with distinct shapes and appropriate d_{hkl} distances. SAED and XRD patterns confirmed crystalline nanoparticles which increase with annealing temperature. XRD analysis also reveals Bragg peaks consistent with Rhombohedral structure of pure α-Cr_2O_3. Raman spectra show A_1g modes at peak position of 547 cm^{-1} identical on all annealed samples. Meanwhile, FTIR spectra present absorption bands at 641 and 632 cm^{-1} which are evidence of the presence of α Cr_2O_3 nanoparticle. Magnetic measurements analysis may indicate that the synthesised Cr_2O_3 nanoparticles are mostly

antiferromagnetic.The optimized geometry, electronic and magnetic properties of antiferromagnetically ordered Cr_2O_3were studied using DFT/GGA level of theory. Our studies indicate that applyinga + U coulomb interaction to the d state of Cr (3 eV) and the p state of O (5 eV) give rise to the best agreement with the experimental observables.

CRediT authorship contribution statement

J. Sackey: Formal analysis, Conceptualization, Experimental sample preparation and analysis, Writing - original draft, Writing - review & editing. **R.Morad:** Formal analysis, Writing - original draft, Computation analysis, writing. **A.K.H. Bashir:** Formal analysis, Writing - original draft, Experimental sample preparation and analysis, Writing. **L.Kotsedi:** Formal analysis, Writing - original draft, Experimental sample preparation and analysis, Writing. **C.Kaonga:** Formal analysis, Sample preparation, Analysis, Writing - review & editing. **M. Maaza:** Supervision, Validation.

Declaration of competing interest

The authors declare that they have no known competing financial interests or personal relationships that could have appeared to influence the work reported in this paper.

Acknowledgement

This work was generously supportedby UNESCO-UNISA Africa Chair in Nanosciences and Nanotechnology (U2ACN2), College of Graduate Studies, University of South Africa, (personnel number 90390490). Facilities required for this work was accessed at iThemba LABS-National Research Foundation. We are also grateful to Nanoscience African Network (NANOAFNET). R. Morad acknowledges the Centre for High Performance Computing (CHPC), South Africa for providing computational resources and facilities for this research project.

References

[1] B.L. Chamberland, The chemical and physical properties of CrO2 and tetravalent chromium oxide derivatives, Crit. Rev. Solid State Mater. Sci. 7 (1) (1977) 1–31.
[2] W.B. White, R. Roy, The system chromium–oxygen at high oxygen pressures, in: Chromium: its Physicochemical Behavior and Petrologic Significance, 1976, pp. 803–817.
[3] K.A. Wilhelmi, At elevated pressures up to 4 kilobar, Acta Chem. Scand. 22 (8) (1968) 2565–2573.
[4] X. Pang, K. Gao, F. Luo, Y. Emirov, A.A. Levin, A.A. Volinsky, Investigation of microstructure and mechanical properties of multi-layer Cr/Cr2O3 coatings, Thin Solid Films 517 (6) (2009) 1922–1927.
[5] M.D. Bijker, J.J.J. Bastiaens, E.A. Draaisma, L.A.M. De Jong, E. Sourty, S.O. Saied, J.L. Sullivan, The development of a thin Cr2O3 wear protective coating for the advanced digital recording system, Tribol. Int. 36 (2003) 4–6.
[6] X. Hou, K.L. Choy, Synthesis of Cr2O3-based nanocomposite coatings with incorporation of inorganic fullerene-like nanoparticles, Thin Solid Films 516 (23) (2008) 8620–8624.
[7] P. Li, H.B. Xu, Y. Zhang, Z.H. Li, S.L. Zheng, Y.L. Bai, The effects of Al and Ba on the colour performance of chromic oxide green pigment, Dyes Pigments 80 (3) (2009) 287–291.
[8] D.W. Kim, S.I. Shin, J.D. Lee, S.G. Oh, Preparation of chromia nanoparticles by precipitation–gelation reaction, Mater. Lett. 58 (12–13) (2004) 1894–1898.
[9] V. Teixeira, E. Sousa, M.F. Costa, C. Nunes, L. Rosa, M.J. Carvalho, J. Gago, Spectrally selective composite coatings of Cr–Cr2O3 and Mo–Al2O3 for solar energy applications, Thin Solid Films 392 (2) (2001) 320–326.
[10] L. Li, Z.F. Yan, G.Q. Lu, Z.H. Zhu, Synthesis and structure characterization of chromium oxide prepared by solid thermal decomposition reaction, J. Phys. Chem. B 110 (1) (2006) 178–183.
[11] Z. Pei, H. Xu, Y. Zhang, Preparation of Cr2O3 nanoparticles via C2H5OH hydrothermal reduction, J. Alloys Compd. 468 (1–2) (2009) L5–L8.
[12] D.W. Kim, S.I. Shin, J.D. Lee, S.G. Oh, Preparation of chromia nanoparticles by precipitation–gelation reaction, Mater. Lett. 58 (12–13) (2004) 1894–1898.
[13] Z.C. Zhong, R.H. Cheng, J. Bosley, P.A. Dowben, D.J. Sellmyer, Fabrication of chromium oxide nanoparticles by laser-induced deposition from solution, Appl. Surf. Sci. 181 (3–4) (2001) 196–200.
[14] T. Tsuzuki, P.G. Cormick, Synthesis of Cr2O3 nanoparticles by mechanochemical processing, Acta Mater. 48 (11) (2000) 2795–2801.
[15] U. Balachandran, R.W. Siegel, Y.X. Liao, T.R. Askew, Synthesis, sintering, and magnetic properties of nanophase Cr2O3, Nanostruct. Mater. 5 (5) (1995) 505–512.
[16] D. Vollath, D.V. Szabó, J.O. Willis, Magnetic properties of nanocrystalline Cr2O3 synthesized in a microwave plasma, Mater. Lett. 29 (4–6) (1996) 271–279.
[17] J. Sackey, A.C. Nwanya, A.K.H. Bashir, N. Matinise, J.B. Ngilirabanga, A.E. Ameh, M. Maaza, Electrochemical properties of Euphorbia pulcherrima mediated copper oxide nanoparticles, Mater. Chem. Phys. (2020) 122714.
[18] M. Bakayoko, F. A, I. Ngom, J. Sackey, B.D. Ngom, P.D. Tall, M. Maaza, Synthesis and characterization of Zinc oxide nanoparticles (ZnO NPs) in powder and in thin film using corn husk extract via green chemistry, MRS Advances (2020) 1–11, https://doi.org/10.1557/adv.2020.98.
[19] A.K.H. Bashir, N. Matinise, J. Sackey, K. Kaviyarasu, I.G. Madiba, L. Kodseti, M. Maaza, Investigation of electrochemical performance, optical and magnetic properties of NiFe2O4 nanoparticles prepared by a green chemistry method, Phys. E Low-dimens. Syst. Nanostruct. (2020) 114002.
[20] M.G. Tsegay, H.G. Gebretinsae, Z.Y. Nuru, Structural and optical properties of green synthesized Cr2O3 nanoparticles, Mater. Today: Proceedings (2020), https://doi.org/10.1016/j.matpr.2020.05.503.
[21] A. Anastácio, R. Silva, I.S. Carvalho, Phenolics extraction from sweet potato peels: modelling and optimization by response surface modelling and artificial neural network, J. Food Sci. Technol. (2016) 4117–4125.
[22] A. Ghasemzadeh, D. Talei, H.Z. Jaafar, A.S. Juraimi, M.T.M. Mohamed, A. Puteh, M.R.A. Halim, Plant-growth regulators alter phytochemical constituents and pharmaceutical quality in Sweet potato (Ipomoea batatas L.), BMC Compl. Alternative Med. 16 (1) (2016) 152.
[23] A.P. Oluyori, A.K. Shaw, G.A. Olatunji, P. Rastogi, S. Meena, D. Datta, S. Puli, Sweet potato peels and cancer prevention, Nutr. Canc. 8 (68) (2016) 1330–1337.
[24] P. Giannozzi, S. Baroni, N. Bonini, M. Calandra, R. Car, C. Cavazzoni, A. Dal Corso, Quantum espresso: a modular and open-source software project for quantum simulations of materials, J. Phys. Condens. *Matter* 21 (39) (2009) 39550.
[25] D. Vanderbilt, Soft self-consistent pseudopotentials in a generalized eigenvalue formalism, Phys. Rev. B 41 (11) (1990) 7892.
[26] J.P. Perdew, J.A. Chevary, S.H. Vosko, K.A. Jackson, M.R. Pederson, D.J. Singh, C. Fiolhais, Atoms, molecules, solids, and surfaces: applications of the generalized gradient approximation for exchange and correlation, Phys. Rev. B 46 (11) (1992) 6671.
[27] J.P. Perdew, K. Burke, M. Ernzerhof, Generalized gradient approximation made simple, Phys. Rev. Lett. 77 (18) (1996) 3865.
[28] J.P. Perdew, A. Ruzsinszky, G.I. Csonka, O.A. Vydrov, G.E. Scuseria, L.A. Constantin, K. Burke, Restoring the density-gradient expansion for exchange in solids and surfaces, Phys. Rev. Lett. 100 (13) (2008) 136406.
[29] V.I. Anisimov, F. Aryasetiawan, A.I. Lichtenstein, First-principles calculations of the electronic structure and spectra of strongly correlated systems: the LDA+ U method, J. Phys. Condens. Matter 9 (4) (1997) 767.
[30] N.J. Mosey, E.A. Carter, Ab initio evaluation of Coulomb and exchange parameters for DFT+ U calculations, Phys. Rev. B 76 (15) (2007) 155123.
[31] S. Shi, A.L. Wysocki, K.D. Belashchenko, Magnetism of chromia from first-principles calculations, Phys. Rev. B 79 (10) (2009) 104404.
[32] A.B. Kehoe, E. Arca, D.O. Scanlon, I.V. Shvets, G.W. Watson, Assessing the potential of Mg-doped Cr2O3 as a novel p-type transparent conducting oxide, J. Phys. Condens. Matter 28 (12) (2016) 125501.
[33] S. Dabaghmanesh, R. Saniz, E. Neyts, B. Partoens, Sulfur-alloyed Cr 2 O 3: a new p-type transparent conducting oxide host, RSC Adv. 7 (8) (2017) 4453–4459.
[34] A. Rohrbach, J. Hafner, G. Kresse, Molecular adsorption on the surface of strongly correlated transition-metal oxides: a case study for CO/NiO (100), Phys. Rev. B 7 (2004) 69, no. 075413.
[35] B. Malki, B. Baroux, O. Le Bacq, A. Pasturel, Density Functional Theory Calculations of Defects Formation Energies in Cr 2 O 3, 2012.
[36] H.J. Monkhorst, J.D. Pack, Special points for Brillouin-zone integrations, Phys. Rev. B 13 (12) (1976) 5188.
[37] A.N. Mallika, A.R. Reddy, K.V. Reddy, Annealing effects on the structural and optical properties of ZnO nanoparticles with PVA and CA as chelating agents, Journal of Advanced ceramics 4 (2) (2015) 123–129.
[38] S. Ananda, N.M.M. Gowda, Synthesis of chromium (III) oxide nanoparticles by electrochemical method and Mukia Maderaspatana plant extract, characterization, KMnO 4 decomposition and antibacterial study, Mod. Res. Catal. 2 (2013) 127, 04.
[39] T. Satgurunathan, P.S. Bhavan, R.D.S. Joy, Green synthesis of chromium nanoparticles and their effects on the growth of the prawn Macrobrachium rosenbergii post-larvae, Biol. Trace Elem. Res. 187 (2) (2019) 543–552.
[40] B.T. Sone, E. Manikandan, A. Gurib-Fakim, M. Maaza, Single-phase α-Cr2O3 nanoparticles' green synthesis using Callistemon viminalis' red flower extract, Green Chem. Lett. Rev. 9 (2) (2016) 85–90.
[41] Z.A. Ahmad, A. Shamim, S. Mahmood, T. Mahmood, F.U. Khan, Biological synthesis and characterization of chromium (iii) oxide nanoparticles, Engineering and Applied Science Letters 1 (2) (2018) 23–29.
[42] C. Ramesh, K. Mohan Kumar, N. Latha, V. Ragunathan, Green synthesis of

Cr2O3 nanoparticles using Tridax procumbens leaf extract and its antibacterial activity on Escherichia coli, Curr. Nanosci. 8 (4) (2012) 603–607.
[43] J. Sackey, M.N.J. Maaza, A. Gibaud, Analysis of the Miscibility of Cd2+ Ions in CaCO3, vol. 17, 2019.
[44] H.C. Barshilia, K.S. Rajam, Growth and characterization of chromium oxide coatings prepared by pulsed-direct current reactive unbalanced magnetron sputtering, Appl. Surf. Sci. 255 (5) (2008) 2925–2931.
[45] J. Mougin, T. Le Bihan, G. Lucazeau, High-pressure study of Cr2O3 obtained by high-temperature oxidation by X-ray diffraction and Raman spectroscopy, J. Phys. Chem. Solid. 62 (3) (2001) 553–563.
[46] M. Balkanski, M. Balkanski (Eds.), Proceedings of the Second International Conference on Light Scattering in Solids, 1971, 1971.
[47] K.F. McCarty, D.R. Boehme, A Raman study of the systems Fe3− xCrxO4 and Fe2− xCrxO3, J. Solid State Chem. 79 (1) (1989) 19–27.
[48] S.H. Shim, T.S. Duffy, R. Jeanloz, C.S. Yoo, V. Iota, Raman spectroscopy and x-ray diffraction of phase transitions in Cr 2 O 3 to 61 GPa, Phys. Rev. B 69 (14) (2004) 144107.
[49] F. Farzaneh, M. Najafi, Synthesis and characterization of Cr2O3 nanoparticles with triethanolamine in water under microwave irradiation, 2001, pp. 329–333.
[50] A.M. Oje, A.A. Ogwu, Chromium oxide coatings with the potential for eliminating the risk of chromium ion release in orthopaedic implants, Royal Society open science, Royal Society open science 4 (7) (2017) 170218.
[51] J. Yang, H. Cheng, W.N. Martens, R.L. Frost, Transition of synthetic chromium oxide gel to crystalline chromium oxide: a hot-stage Raman spectroscopic study, J. Raman Spectrosc. 42 (5) (2011) 1069–1074.
[52] M.K. Trivedi, R.M. Tallapragada, A. Branton, D. Trivedi, G. Nayak, O. Latiyal, S. Jana, Characterization of physical, thermal and structural properties of chromium (VI) oxide powder: impact of biofield treatment, Powder Metallurgy & Mining 4 (1) (2015). OMICS Publishing Group.
[53] J. Sackey, A.K.H. Bashir, A.E. Ameh, M. Nkosi, C. Kaonga, M. Maaza, Date pits extracts assisted synthesis of Magnesium Oxides Nanoparticles and its application towards the photocatalytic degradation of methylene blue, J. King Saud Univ. Sci. (2020), https://doi.org/10.1016/j.jksus.2020.06.013.
[54] A.C. Santulli, M. Feygenson, F.E. Camino, M.C. Aronson, S.S. Wong, Synthesis and characterization of one-dimensional Cr2O3 nanostructures, Chem. Mater. 23 (4) (2011) 1000–1008.
[55] M. Feygenson, A. Kou, L.E. Kreno, A.L. Tiano, J.M. Patete, F. Zhang, M.C. Aronson, Properties of highly crystalline NiO and Ni nanoparticles prepared by high-temperature oxidation and reduction, Phys. Rev. B 81 (1) (2010), p. 014420.
[56] A.K. Bashir, M.B.T. Tchokonté, A.M. Strydom, Electrical and thermal transport properties of RECu4Au compounds, RE= Nd, Gd, J. Magn. Magn Mater. 414 (2016) 69–73.
[57] A.K. Bashir, M.B.T. Tchokonté, D. Britz, B.M. Sondezi, A.M. Strydom, Magnetic and thermodynamic properties of GdCu4Au, Conference Series IOP Publishing, J. Phys. 592 (1) (2015), p. 012050.
[58] P.J. Brown, J.B. Forsyth, E. Lelièvre-Berna, F. Tasset, Determination of the magnetization distribution in Cr2O3 using spherical neutron polarimetry, J. Phys. Condens. Matter 14 (8) (2002), p. 1957.
[59] A. Rohrbach, J. Hafner, G. Kresse, Ab initio study of the (0001) surfaces of hematite and chromia: influence of strong electronic correlations, Phys. Rev. B 70 (12) (2004) 125426.